Materials Research Express

PAPER

Orthorhombic molybdenum trioxide micro-planks as carbon monoxide gas sensor

To cite this article: Dharma K Halwar *et al* 2019 *Mater. Res. Express* **6** 105913

Materials Research Express

PAPER

Orthorhombic molybdenum trioxide micro-planks as carbon monoxide gas sensor

Dharma K Halwar[1], **Vikas V Deshmane**[2,4] **and Arun V Patil**[3]

[1] Thick and thin film laboratory, M.S.G. College, S P Pune University, Malegaon, Maharashtra, India
[2] SICES Degree College of ASC, University of Mumbai, Ambarnath, Maharashtra, India
[3] Research center in electronics,LVH College, S P Pune University, Nashik, Maharashtra, India
[4] Author to whom any correspondence should be addressed.

E-mail: halwardk9@gmail.com, desh8299vv@gmail.com **and** aruptl@gmail.com

Keywords: Molybdenum trioxide, Micro-planks, Copper, Surface oxygen hopping, Carbon monoxide

RECEIVED
9 May 2019

REVISED
9 August 2019

ACCEPTED FOR PUBLICATION
1 September 2019

PUBLISHED
11 September 2019

Abstract

Study was aimed at analyzing gas sensing properties of copper oxide doped molybdenum trioxide. Screen printing method was used to prepare thick films of five different weight percent of copper oxide. XRD confirmed that material consists pure alpha phase of ortho-rhombic molybdenum trioxide (JCPDS 21-0569). FE-SEM micrographs showed plank-like structure having all three dimension in microns. Hence authors used term micro-planks. EDS analysis showed that all sample were having excess oxygen. Electrical measurement showed n-type semiconductor behavior of films. TCR also showed negative values for all films. Resistivity of the films reduced from 80 Ω m to 25 Ω m as copper oxide percentage increased. Activation energy in high temperature region also decreased from 0.6 eV to 0.25 eV due to addition of copper oxide dopant. 9 Wt% copper added molybdenum trioxide films (Cu9) showed 74.87% response to carbon monoxide gas at 150 °C. Response time (80 s) and recovery time (110 s) was quick. The synergy between thermal energy, oxygen excess samples, the activity of micro-planks and catalytic property of copper oxide dopant accelerated the reduction of carbon monoxide. Hence selectivity to carbon monoxide gas as compared with NH_3, NO_2, Ethanol vapor and LPG improved due to copper oxide dopant.

1. Introduction

Metal oxide semiconductors (MOS) have been studied for many years. Divergent properties made MOS useful in many applications. Molybdenum trioxide (MoO_3) is one of the many n-type MOS. MoO_3 has phases like alpha and beta. The beta phase of MoO_3 is vulnerable to the surrounding conditions. The alpha phase of MoO_3 is a relatively more stable phase. MoO_3 has a lower transition temperature, above which only the stable alpha phase of the MoO_3 exists. MoO_3 has a tendency to form a lamellar structure [1].

The lamellar structure of MoO_3 has been used in lubricant application. Addition of dopants increased the load-bearing capacity of the lubricant MoO_3 [2]. Electrochromic systems such as smart windows, optical displays utilized switchable transparency of MoO_3 in presence of positive ions [3]. MoO_3 has also been used for designing field effect transistors (FET) [4]. MoO_3 with graphite coating has been used as a battery electrode [5]. Organic light emitting diodes (OLED) and organic photovoltaics (OPV) also use MoO_3 [6].

Role of Molybdenum trioxide as a gas sensor has been studied by many research group using various synthesis methods and diverse testing conditions. The surveyed literature has been summarized in table 1. Pristine and doped molybdenum trioxide has responded to organic compound vapors and hazardous gases. The operating temperature was slightly higher. Response and recovery time was also quick for all the surveyed literature. Complex synthesis methods have been adopted, which have lower reproducibility. In the current study, the simplest method of screen printing was adopted to ensure the reproducibility of the sensor. Authors wanted to utilize the catalytic property of copper oxide towards the reduction of carbon monoxide and other hazardous gases. Hence study used copper oxide as a dopant.

Table 1. Summary of literature survey for MoO_3 as a gas sensor.

Material and dopant	Synthesis	Sensitivity parameters	Operating temp., response and recovery time	References
MoO_3	Situ Diffusion Growth	Tri-methyl amine (100 ppm) 104.8% (Ra/Rg)	280 °C	[7]
$CoMoO_4$-MoO_3			220 °C	
ZnO –CuO nanoflakes	RF diode sputtering	Acetone (5 ppm)	300 °C	[8]
		52.7%	Rs 22 s	
MoO_3 + Au	Evaporation	H_2S (15 ppm)	400 °C	[9]
Dopant gold	Condensation	250% (Ra/Rg)		
Ru-MoO_3	Hydrothermal	H_2S (10 ppm)	350 °C	[10]
Nano flakes	Route	30%		
MoO_3	Hydrothermal	H_2 (1000 ppm)	300 °C	[11]
Nano ribbons		17%	Rs 11 s and Rc 31 s	
MoO_3 Nanorads	Infrared Irradiation Heating	CO (100 ppm) 50%	200 °C	[12]
MoO_3 Nanorads	SG and RFSputerring	CO (500 ppm) 30%, RF	300 deg 300 ppm	[13]
	500 deg annealing	SG	Rs 100 s and Rc 100 s Rs 50 s and Rc 100 s	
MoO_3 + TiO_2	Sol-Gel Thin films	CO (400 ppm) 2.9% NO_2 (20 ppm) 2.7%	300 °C Rs 2 min and Rc 3 min	[14]
CuO Nanotube CuO Nanocubes	Sol-gel and annealing	CO (1000 ppm)	175 °C Rs 29 s Rc 37 s Rs 11 s and Rc 18 s	[15]
MoO_3	RF Magnetron Sputtering in Ar/O_2 atmosphere and annealed at 500 deg	NO_2 (10 ppm)	300 °C	[16]
Thin film			Rs 120 s and Rc 420 s	
MoO_3	ION beam deposited SolgelCalcination 500 deg.	NO_2 (200 ppm) NH_3 (200 ppm)	450 °C Rs few sec Rc 2–3 min 500 °C Rs 20–30 s and Rc 5–7 min	[17]
MoO_3	Thermal Evaporation	NO_2(10 ppm) 118% (Ra/Rg)	225 °C	[18]
ZnO/CuO Compo. Al dopant	Co-precipitation followed by sol-gel	NH_3 (500 ppm)	Room Temp Rs 14 s and Rc 9 s	[19]
Graphene Oxide CuO dopant	Modified hummer method and annealing	NO_2 (20 ppm)	190 °C	[20]

The research was aimed to study the effect of copper oxide on the structural, electrical and elemental composition of molybdenum trioxide films. The study also tried to relate the gas sensing performance of molybdenum trioxide with the above-mentioned properties.

2. Experimental methods

All the chemicals of AR grade without further purification were used for the study. Thick films of Molybdenum Trioxide with copper oxide as an additive were prepared using standard screen printing setup. Paste preparation was the first important part of the film preparation. Glass frit was used as a permanent binder between base material, dopant and alumina substrate. Ethyl cellulose performed the role of a temporary binder. Butyl Carbitol Acetate (BCA) was used to make a paste with proper thixotropic properties.

Inorganic and organic materials were used in 70:30 weight percent ratios. Inorganic material consisted of the base material (Molybdenum Trioxide) and dopant (Copper). Molybdenum trioxide and copper were taken in 99:1, 97:3, 95:5, 93:7 and 91:9 weight percent ratios. Corresponding prepared films were termed as Cu1, Cu3,

Cu5, Cu7, and Cu9 respectively in further communication. We didn't take further Wt% of dopants because we wanted to study and modify the gas sensing properties of the base material (Molybdenum Trioxide) with a minimum proportion of dopant (Copper). If dopant percentage was higher, Copper properties would have dominated the Molybdenum Trioxide properties. Organic material (30 Wt%) consisted of 8% Ethyl Cellulose, 84% Glass frit and a few drops of Butyl Carbitol Acetate (BCA). All of the properly weighed materials were mixed and crushed in mortal pastel for about 30 min few drops of BCA were added to make proper thixotropic paste.

Nylon screen (120 mesh) with scientifically developed 1.25 cm × 2.50 cm window was used for film preparation. Alumina sheet cleaned with double distilled water was used as a substrate for the films. The pre-prepared paste was applied on the screen. Uniform pressure was applied on the squeeze, which pressed the paste through nylon screen pours onto the alumina substrate. This was the screen printing method used to prepare the films. Films were allowed to settle down for 15 min. The prepared films were dried under an IR lamp for 15 min. The temporary binder evaporated during this irradiation process. It was well known that below 350 °C multiple phases of molybdenum trioxide exist. These phases are vulnerable to the changes in the surrounding. Beyond 500 °C only alpha phase of molybdenum trioxide (α-MoO_3) exists. The α-MoO_3 has long range stability. Hence the films were annealed at 600 °C in a furnace with air atmosphere. Films were found to be well adherent to the substrate.

The films were then characterized using x-ray diffractometer (XRD) (D8 Advance, Bruker-AXS), field effect scanning electron microscope (FE-SEM) (FEI-Nova Nano SEM 450), and energy dispersive spectrometer (EDS) (Bruker XFlash 6I30) at S. P. Pune University. Electrical and gas sensing measurement was carried out using a static gas sensing apparatus. This apparatus consisted of a serial arrangement of a known resistor and sample to be tested. Constant DC voltage (Aplab) was applied across the above series arrangement. The heater was placed below the sample to be tested. The whole assembly was placed in a glass chamber of volume 20 liters. The temperature inside the chamber was controlled using a dimmer stat attached to the heater. Chrome/Alumel (K-type) calibrated thermocouple was used to measure the temperature. Gases were injected into the chamber using micro-syringes. The thickness of the sample (20 μm) was measured using standard BET method.

For sample with length (l), breadth (b), thickness (t) and resistance (R), resistivity was calculated using formula,

$$\rho = (R^*b^*t)/l(\Omega.\mathrm{m}) \tag{1}$$

Temperature coefficient of resistance (TCR) of the sample having room temperature resistance (R0), change in resistance (ΔR) and a corresponding change in temperature (ΔT) was calculated using the following formula [21],

$$TCR = (1/R_0)(\Delta R/\Delta T)\ (\text{per degree Kelvin}) \tag{2}$$

Resistance (R) at temperature (T) are related by Arrhenius equation as follows [22],

$$R = R_0 \exp(-\Delta E/kT) \tag{3}$$

Here R_0 is the room temperature resistance, ΔE is the activation energy and k is Boltzmann constant.

Percentage sensitivity of sample with resistance in the air (R_a) and resistance in gas (R_g) was calculated using formula,

$$\%S = \left| \frac{R_a - R_g}{R_a} \right| x100 \tag{4}$$

The selectivity of films plays an important role in sensors properties. If $S_{\text{target gas}}$ is the sensitivity of sample to target gas and $S_{\text{other gas}}$ is the sensitivity of sample to other gas then selectivity was calculated using the following formula [23],

$$\%Selectivity = (S_{targetgas}/S_{othergas})x100 \tag{5}$$

3. Results and discussion:

3.1. XRD

It is necessary to verify the content of the sample, its crystallinity and structural parameters to get an insight into films material. Hence films of Cu1, Cu3, Cu5, Cu7 and Cu7 samples were characterized using XRD. XRD plots have been showcased in figure 1. The peaks were observed at 2 theta positions of 13.12, 23.72, 26.04, 30.02, 39.35, 40.05, 57.86, 59.21, 65.2 and 67.85. All of these peaks perfectly matched with JCPDS card no.21–0569. The planes corresponding to the peaks were aligned along [110], [200], [210], [204], [224], [320], [218], [424], [610] and, [524] direction. Our sample was proved to be α-MoO_3 having orthorhombic structure. No peaks corresponding to other phases of molybdenum oxide were observed. β-MoO_3 phase is temperature dependent.

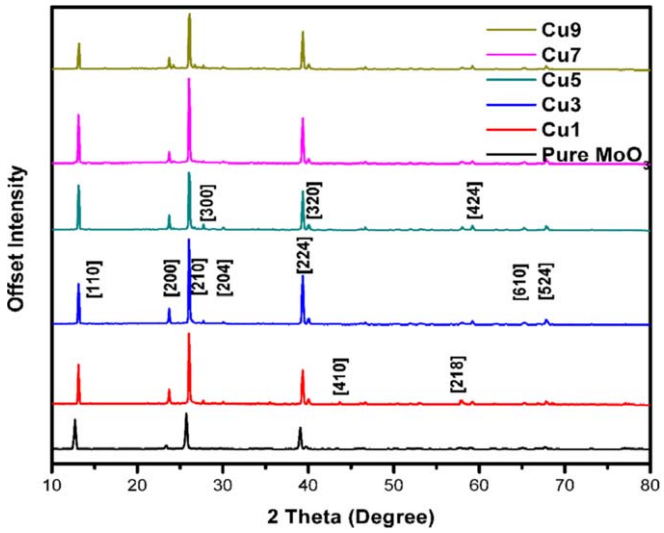

Figure 1. XRD stack of undoped. Cu1, Cu3, Cu5, Cu7 and Cu9 films.

Hence the purity of the samples was also established. This purity of α-MoO_3 affirmed long term stability and response of the sample. Three of the major peaks were along [110], [210] and [224]. Most preferred orientation was along [210] direction. This proved anisotropic growth of the crystals.

As per Epifani *et al*, mixed α and β phases of MoO_3 at lower temperature got transformed into pure α phase of MoO_3 after annealing beyond 350 deg. Celsius. Samples in the current study have been annealed at 600 °C hence it is obvious that we should get the pure alpha phase of molybdenum trioxide [24].

Crystallite size was calculated using x-powder 12 software. Crystallite size was calculated by taking an average of the three most intense peaks. It was found to have an average crystallite size of 50 nm. The intensity of the preferred peaks was increasing with the increase in doping percentage. This meant that crystallinity also increased with the rising in dopant percentage. Peaks corresponding to dopant (Cu) were not observed in the XRD plot due to less percentage of copper oxide.

The target of the study was to analyze the effect of copper on the gas sensing properties of base material i.e. molybdenum trioxide. This meant that major role should be of base material and dopant should be only in modifier role. The aim of the study was cemented by the dominant presence of MoO_3 and negligible less presence of copper oxide according to XRD plot.

3.2. SEM

The morphology and surface analysis of constituents can be studied through field effect scanning electron microscope (FESEM) images. FESEM images of the Cu1, Cu3, Cu5, Cu7 and Cu7 samples have been shown in figures 2(a)–(e). Figure 2(f) shows the characteristic shape of dopant (Cu) particles.Molybdenum trioxide particles show characteristic lamellar structure. The agglomerated particles have formed wooden plank like structure. All dimensions of the agglomerate were in the micrometer range. Hence we call the structure as micro-planks. The thickness of the micro-planks was in the range of 1 to 1.8 microns range. The width of the micro-planks was less than 7.32 micron. The micro plank of length 31.13 microns was observed in the scanned area. At 5k magnification, the surface of the micro-planks was observed to be quite uniform. The end of the micro-planks was rounded but with uniform thickness. Very clear boundaries of the planks were observed. Gaps were observed between the planks.

As explained by Epifani *et al* (2014), during the synthesis of MoO_3 films, extensive hydrolysis of the molybdenum precursor tends to a highly cross-linked structure. The lamellar structure of base material molybdenum trioxide in the current study can be understood with the preference to form crosslinks. Large domain structures within molybdenum trioxide also favor lamellar surface structure [24].

These type of agglomerates have a lesser surface to volume ratio as compared to mesoporous films. The internal region of the micro-plank remains totally isolated from the surrounding. The higher temperature must be employed to interact with the internal structure of the micro-plank. In order to enhance interaction between sample content and surrounding the plank thickness should be reduced using various synthesis parameters. Few atomic layers thick planks (nano planks) would be very productive for various application.

The screen printing method used in the current study can be proved to be very useful in controlling dimensions of the micro-planks. Currently, authors have used nylon screen of 120 mesh which corresponds to

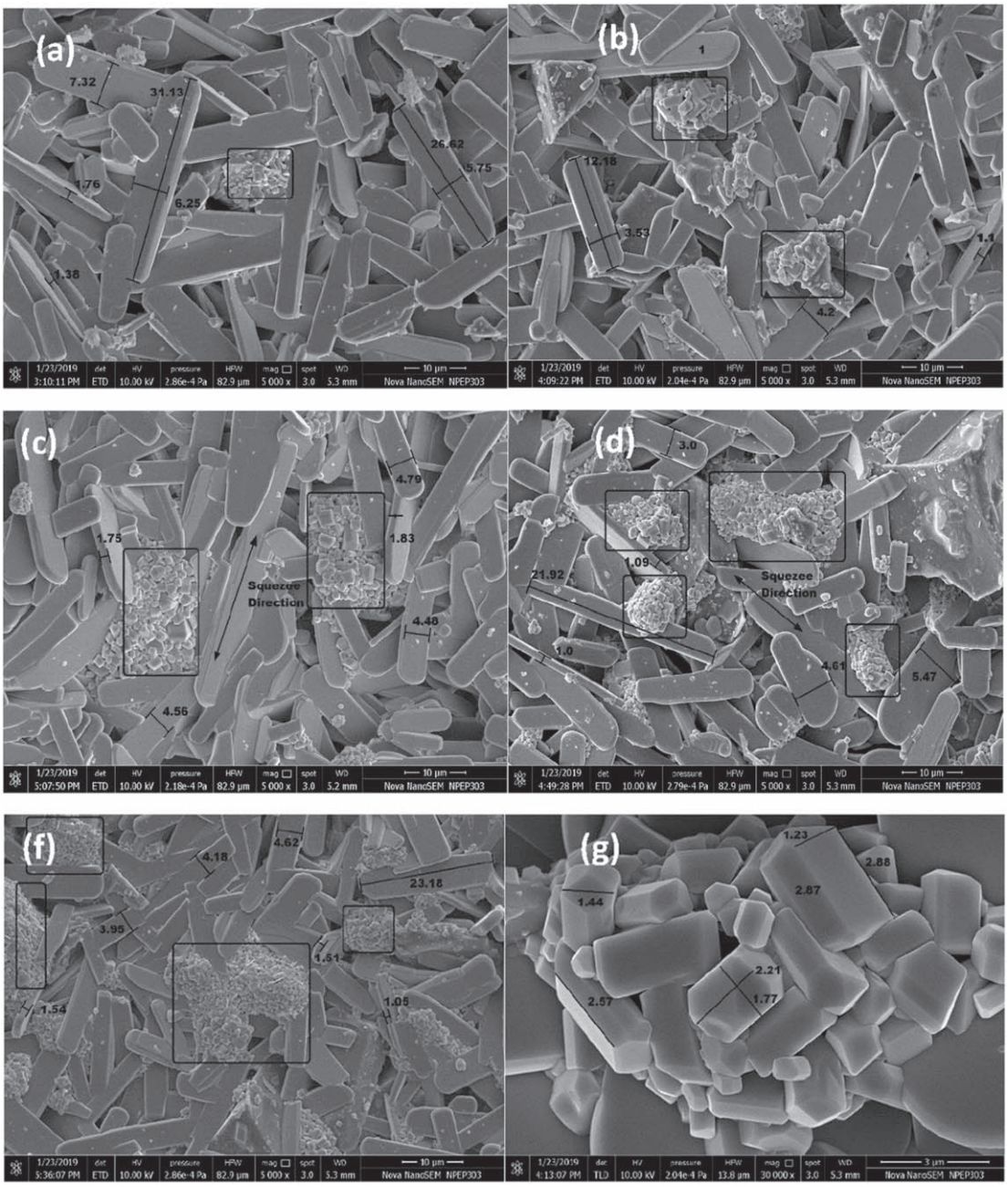

Figure 2. SEM micrographs of (a) Cu1, (b) Cu3, (c) Cu5, (d) Cu7, (e) Cu9 and (f) dopant particles observed in Cu9.

pore (sieve) of size 125 micron. As observed in SEM this setup has produced micro-planks of few microns dimensions. If higher mesh sized nylon screens (i.e. lower sieve size) and finely prepared materials are used, definitely thinner and slender micro-planks can be prepared. When the paste is applied on the screen surface and pressed via squeeze. The direction of the squeeze motion determines the direction of the laid micro-planks. The pressure of the squeeze determines the thickness of the micro-planks. This method is definitely cheaper, portable, easier and reproducible for preparing molybdenum trioxide micro-planks.

Black rectangular box showcased the dopant (i.e. copper) distribution. The dopant particles were very small as compared to the micro-plank dimension. As dopant weight percentage increased the planks were found to be lesser in length as observed in figures 2(d) and (e). This shortening of lengths of micro-planks can be attributed to discontinuity introduced by the dopants during agglomerations. The dopant ruptures the cohesive forces between neighboring molybdenum molecules to break the agglomeration continuity.

Dopant particles also introduce irregularities along the surface of molybdenum trioxide micro-planks. These irregularities increase the surface to volume ratio and inter-particle voids. Higher surface to volume ratio and inter-particle voids facilitate oxygen/target gas adsorption.

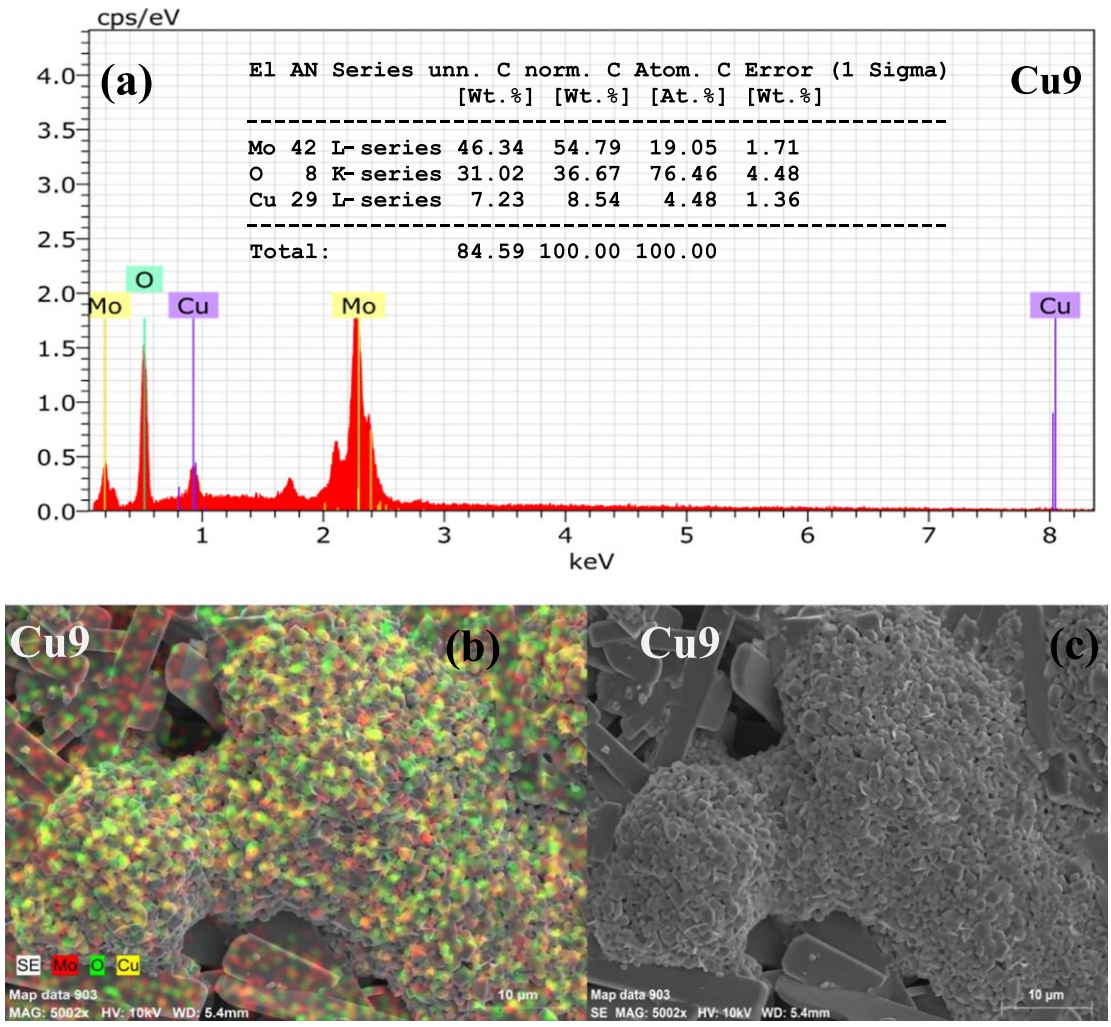

Figure 3. (a) EDS spectra of Cu9 sample, (b) colored elemental distribution in Cu9, (c) non-colored image of figure 3(b).

Dopant was distributed non-uniformly over the base material. This is one of the disadvantages of the mechanical mixing method used for doping. Proper care must be taken while mixing and crushing the mixture in mortal pastel. Therefore while studying electrical parameters, the testing cycles must be repeated and averaged out.

3.3. EDS

The presence of dopant and elemental distribution of the thick film constituents can be re-confirmed using energy dispersive study (EDS). All Cu1, Cu3, Cu5, Cu7 and Cu7 samples were characterized using EDS. Representative spectra of Cu9 sample was shown in figures 3(a). Figure 3(b) and (c) show colored and non-colored elemental distribution as per EDS analysis.If one molybdenum trioxide and one copper oxide molecules are considered then Mo: O: Cu atomic ratio should be 1:4:1. The study used very less weight percentage of copper. Comparatively the films were observed to have excess oxygen as per table 2. This excess oxygen must be adsorbed during calcination. Colored elemental mapping admitted that the smaller sized particles correspond to dopants (copper). Certain minor peaks observed in EDS spectra can be attributed to the constituents of the alumina substrate.

3.4. Electrical characteristics

Figure 4(a) showed the changes in the resistance of Cu1, Cu3, Cu5, Cu7 and Cu9 thick films with the varying temperature at the interval of 10 °C. Electrical measurements have been repeated three times. Averages values of the three cycles have been showcased as final measurements in figure 4(a).

It can be easily observed that as temperature increased the resistance of all samples decreased. According to the change in resistance with varying temperature, semiconductors are divided into two categories. Semiconductor whose resistivity decreases with increase in temperature has a negative temperature coefficient

Table 2. Elemental distribution in Cu1, Cu3, Cu5, Cu7 and Cu9 samples

Element	Atm. No.	Cu1		Cu3		Cu5		Cu7		Cu9	
		Wt%	At%	Wt%	At%	Wt%	At%	Wt%	At%	Wt%	At%
Mo	42	60.81	20.71	59.75	20.40	58.45	19.97	56.09	19.04	54.79	19.05
O	8	38.71	79.05	38.41	78.65	38.22	78.31	38.38	78.12	36.67	76.46
Cu	29	0.48	0.25	1.84	0.95	3.32	1.71	5.53	2.83	8.54	4.48

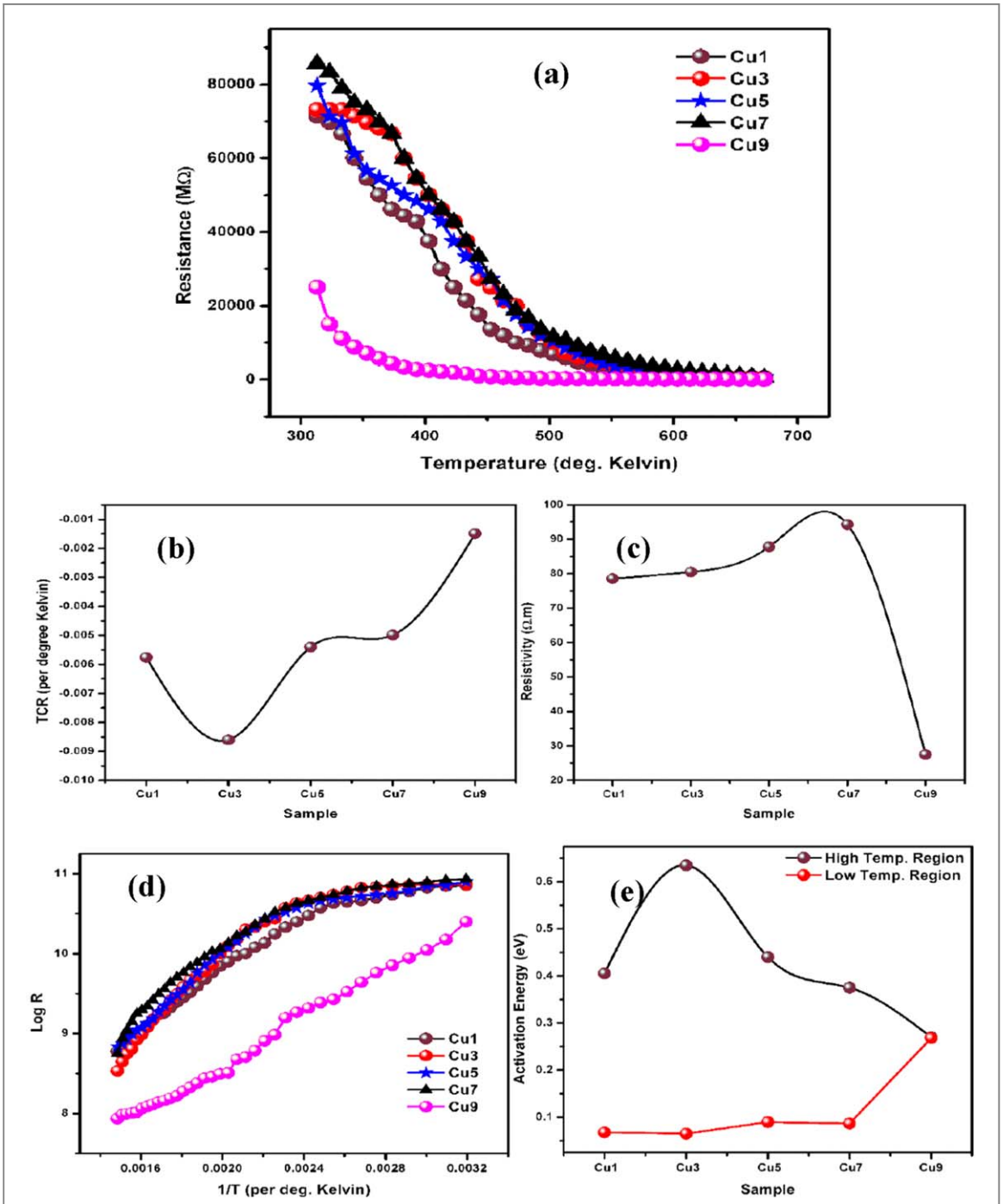

Figure 4. Variation of (a) resistance versus temperature, (b) TCR, (c) resistivity, (d) logarithm of resistance with inverse temperature and (e) activation energy in high and low temperature region for Cu1, Cu3, Cu5, Cu7 and Cu9 samples.

and called an n-type semiconductor. If resistance increases with increase in temperature the semiconductors have a positive temperature coefficient of resistance. All five samples showed negative value for temperature coefficient of resistance (TCR). Hence we can say that the samples behaved like an n-type semiconductor. N-type

semiconductors have negative charge carriers. Here the charge carriers could be electron or O^- ions. O^- Ions can be formed due to the high electron affinity of oxygen during adsorption [25].

Cu1, Cu3, Cu5 and Cu7 samples followed the almost same trend in resistance fall. Room temperature resistance of these samples was in several thousand megaohms. At the start of the cycle, the resistance decreased suddenly and after about 550 °Kelvin these four samples achieved minimum resistance value. But the trend followed by Cu9 sample was very different. Room temperature resistivity of the Cu9 sample was nearly one-fourth of the maximum resistivity value as per figure 4(b). A lower limit for resistance was achieved at 425 °C only. This variation in resistance trend must be due to the addition of copper (Cu). Trend of TCR was shown in figure 4(c).

Figure 4-d is the Arrhenius plot, a graph of the logarithm of resistance versus temperature^{-1}. It can be easily seen that these graphs for Cu1, Cu3, Cu5 and Cu7 sample have two distinct regions. One region is the rising region called a high-temperature region. After a particular transition temperature, the graph shows a very small variation in resistance. This region of the nearly horizontal line is called a low-temperature region. The Arrhenius plots were used to calculate the activation energy of the samples. Figure 4-eindicates the variation of activation energy in the low and high-temperature region. In the low-temperature region, the variation in activation energy was very small.

As the temperature was varied during the experiment, it meant that the thermal energy supplied to the sample elements was varied. This thermal energy causes atoms/molecules to move from lower energy levels to higher energy levels. If this supplied energy is greater than or equal to the binding energy of the electrons, then electrons take part in conduction. It is interpreted as an increase in conductivity or conversely decreases in resistivity. The energy required for this transition is the activation energy.

As explained by Rosso *et al* (2003) activation energy can be understood using the Franck Condon principle and small polaron model. For an electron to move from one lattice site to the next lattice site, the energy levels of both the sites must be comparable. Thermal fluctuations reorganize energy levels of both sites, to facilitate electron transfer. This is the activation energy required for an electron to hop from one lattice site to another. Continuous hopping forms the conduction process. In short activation energy is reorganization energy that mediates between reactants and products [26].

It was obvious that in the low-temperature region sufficient energy was not available for the electron to overcome the potential barrier. Due to the addition of copper the activation energy for Cu5 sample was found to be lowest. This meant that the electron conduction could appear with relatively low thermal energy. This made Cu5 sample, a good candidate for gas sensing application. As copper weight percentage increased beyond 7% the activation energy increased. Copper when heated in air atmosphere at 600 °C forms copper oxide. This increase in activation energy must be due to p-type behavior of CuO. At lower weight % it didn't affect the carrier concentration. As the p-type material increased it obvious that the negative charge carriers would be attracted towards p-type material. Hence available charge carriers get reduced and conductivity of the sample decreases. Lesser was the conductivity more would be the energy required to overcome the potential barrier.

Figure 4-dshowed almost linear variation in the resistance of the Cu9 sample. It indicated a shift in the performance of the Cu9 sample from semiconductor behavior. Therefore we didn't test further dopant percentages. Here the copper properties started to dominate the base material properties. We know that copper is a very good conductor of electricity. Hence almost linear variation in resistance was observed. This behavior can be attributed to the dominant catalytic nature of copper oxide as explained by J. Singh *et al* (2016) and W. Wang (2015) [27, 28].

3.5. Gas sensing

The gas sensing performance of Cu1, Cu3, Cu5, Cu7, and Cu9 samples have been showcased in figures 5(a)–(d) respectively. All of the above samples showed a very good response to carbon monoxide gas. As copper weight percentage increased, the percentage sensitivity of the samples towards carbon monoxide gas also increased. The response to all other tested gas was relatively lower. The optimum temperature for each of the tested sample was about 150 °C–200 °C. Optimum temperature is the temperature at which supplied thermal energy is just sufficient for valence band electron to enter into the conduction band.

At the beginning all of the samples were tested for 1000 ppm of target gas. Cu1 sample showed a sensitivity of 34% to both carbon monoxide and ethanol vapor at 150 °C. The selectivity between carbon monoxide and ethanol was negligible. This is not the desired quality for good gas sensor. As the weight percent of the copper additive increased the selectivity towards carbon monoxide was improved. Conversely, sensitivity to ammonia decreased with increase in dopant percentage.

Cu3 films showed 37% sensitivity to carbon monoxide gas at 200 °C. Cu5 films displayed 50% sensitivity to carbon monoxide (CO) at 200 °C. Cu7 films presented 50% sensitivity towards CO at 150 °C. Selectivity for

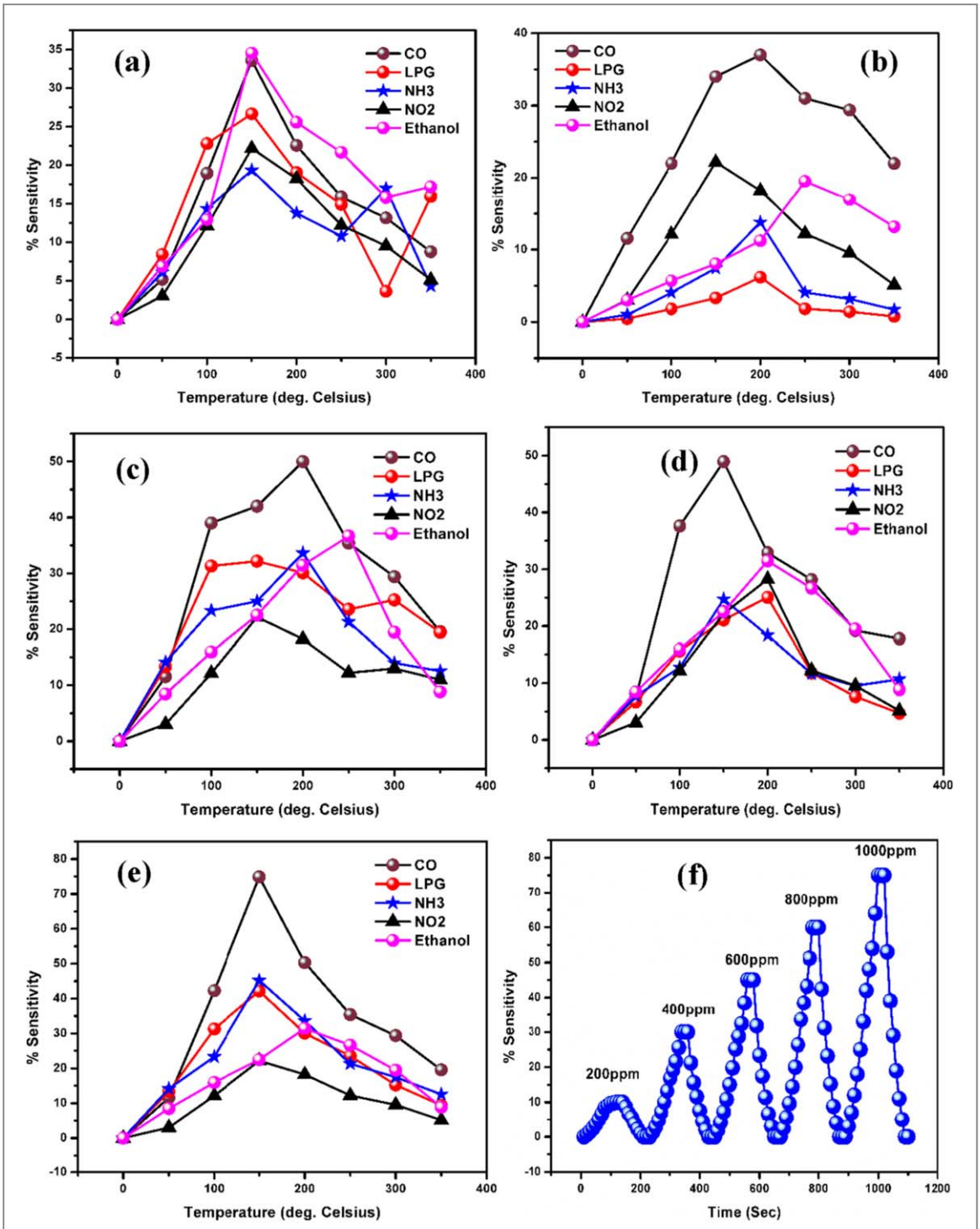

Figure 5. Sensitivity versus temperature for (a) Cu1, (b) Cu3, (c) Cu5, (d) Cu7, (e) Cu9 and (f) sensitivity versus time for various CO gas concentration in ppm.

carbon monoxide gas w.r.t. ammonia, ethanol vapor, LPG and nitrogen dioxide was maximum for Cu9 films. Sensitivity towards CO gas (1000 ppm) was 74.89%.

Variation of the sensitivity of Cu9 films with CO gas concentration was studied. Corresponding response and recovery time for gas sensing has been demonstrated in figure 5(e). It clearly showed that with increased target gas concentration sensitivity also increased. It was obvious that with the increase in gas concentration, more target gas was available for interaction. More gas meant more probability of adsorption and sensitivity improved.

Response time was the time taken by the sample to reach 90% of its maximum sensitivity value when gas was inserted into the chamber. Recovery time was the time taken to reduce to 10% of the maximum sensitivity value

when target gas was turned off. Cu9 films presented a quick response time of 80 s and recovery time of 100 s at 150 °C.

3.6. CO sensing mechanism

Combustion processes in industries and automobiles generate hazardous gases. Carbon monoxide is one of the major air pollutants. When carbon monoxide reacts with hemoglobin in human blood, the oxygen-carrying capacity of the blood decreases. Excessive exposure to carbon monoxide can also cause death. Hence CO sensing has its importance in the modern industrial era. [29].

Molybdenum trioxide micro-planks and copper dopant cordially improved CO gas sensitivity and selectivity. Various studies have proposed multiple gas sensing mechanisms. One of the common explanation can be given using adsorption and desorption mechanism. Oxygen has a greater electron affinity. Oxygen ions in molecular form (O^{2-}) or atomic form (O^{-}, O^{2-}) get adsorbed on the micro-plank surface of MoO_3. The molecular form of oxygen ion has relatively lower activation energy at a higher temperature. Hence the adsorption of molecular oxygen ions was more probable at higher temperatures [30]. MoO_3 is a normal n-type semiconductor. Comini *et al* proposed that when CO is introduced in the gas chamber, the exchange of electrons takes place between the semiconductor and ionosorbed oxygen species causing a change in resistance [12].

Some reports proposed that it was not the adsorbed oxygen but the lattice oxygen that played a major role in gas sensing. Oxygen present at lattice sites oxidized the target gas molecule catalytically. After desorption of the target gas molecules, the oxygen vacancies were created at the surface of the base material. These oxygen vacancies at the surface were fulfilled by the oxygen in the inner region of the micro-planks. This process caused changes in the conductivity of the base material [30].

Copper oxide is well known for its catalytic applications. Huang *et al* (2003) have stated that copper oxide has the special property of surface lattice oxygen hopping. Ability to capture and release surface oxygen during the reduction of target gas which makes copper oxide a good catalyst in carbon monoxide reduction. Huang *et al* stated Mars-van Krevelen redox reaction for the reduction of carbon monoxide. Here O_{SL} was the surface lattice oxygen and O_{SV} was the oxygen vacancy on the surface lattice. [12]

$$CO + O_{SL} \rightarrow CO_2 + O_{SV} \tag{6}$$

$$O_2 + O_{SV} \rightarrow 2O_{SL} \tag{7}$$

Reaction (6) was the reduction rate determining step which removes oxygen from the CuO surface. Reaction (7) was re-oxidation of the catalyst surface, it was relatively fast. In oxygen-rich condition, this catalytic reaction is completed more speedily. According to EDS analysis (table 2) of the current study, the samples were excess in oxygen, which facilitated the reduction of carbon monoxide.

Copper remained inactive up to 140 °C and beyond 140 °C its activity increased as per Huang *et al* [12]. This clearly matched with our transition temperature in the Arrhenius plot (figure 4(d)) and optimum gas sensitivity temperature of 150 °C (figure 5(d)). The synergy between thermal energy, oxygen excess samples, the activity of micro-planks and catalytic property of copper oxide dopant accelerated the reduction of carbon monoxide. This increased the sensitivity and selectivity to CO gas. Faster reduction of target gas also reflected in relatively lower response (80 s) and recovery time (110 s)(figure 5(e)).

4. Conclusion

In the current study, authors put forth screen printing method for production of micro-planks (can be called multi-layered nano-belts) of molybdenum trioxide. The study proposed cost-effective, portable, reproducible MoO_3 micro-planks synthesis. Further experiments on controlling dimensions of micro-planks using higher mesh nylon screen for screen printing needs to be done.

XRD confirmed that films constituted pure alpha phase of MoO_3 which has long term stability.This stability property made alpha-MoO_3 (base material) a good candidate for stable gas sensor purpose. Negative TCR of samples proposed n-type semiconductor behavior of all films. As the dopant percentage increased the resistivity and activation energy (in the high-temperature region) of the samples decreased. Cu9 films showed minimum resistivity and activation energy. EDS conveyed that all the films were having excess oxygen.

Static gas sensing study conveyed that the Cu9 samples showed the highest sensitivity (74.89%) to carbon monoxide gas at 150 °C. Selectivity to CO gas was very good as compared to other tested gases. Response (80 s) and recovery (100 s) time were also quick. Surface oxygen hopping model proposed in Mars-van Krevelen redox reaction was found suitable to explain the gas sensing mechanism. The collective effect of supplied thermal energy, oxygen excess species, the activity of micro-planks and catalytic property of copper dopant made Molybdenum oxide good carbon monoxide sensor.

Further research can be done on controlling micro-planks dimensions using simple and reproducible screen printing method.

Acknowledgments

Authors would like to acknowledge Principal, MSG College, Malegaon and Principal LVH College, Nasik, for providing necessary research facility. Authors would also like to thank Dept. of Physics and Central Instrumentation Facility at S P Pune University for providing characterization facility.

Conflict of interest

Authors declare no conflict of interest.

Funding

Authors received no funding for current research study.

ORCID iDs

Vikas V Deshmane https://orcid.org/0000-0001-6351-4162

References

[1] Sun S P, Zhu J L, Gu S, Li X P, Lei W N, Jiang Y and Chen G H 2018 First principles investigation of the surface stability and equilibrium morphology of MoO_3 *Appl. Surf. Sci.* **467–468** 753–59
[2] Gulbiński W and Suszko T 2006 Thin films of MoO_3–Ag_2 O binary oxides – the high temperature lubricants *Wear* **261** 867–73
[3] Olayinka O, Mengmeng K, Kalulu M, Fang Y and Guodong F 2018 Facile synthesis and study of the photochromic properties of deep eutectic solvent-templated cuboctahedral-WO_3/MoO_3 nanocomposites *Superlattices Microstruct.* **125** 103–112
[4] Ren Z, Zhang J, Zhang J, Zhang C, Yang P, Chen D and Hao Y 2018 Research on the hydrogen terminated single crystal diamond MOSFET with MoO3 dielectric and gold gate metal *J. Semicond.* **39** 074003
[5] Tojo T, Tawa H, Oshida N, Inada R and Sakurai Y 2018 Electrochemical characterization of a layered α-MoO_3 as a new cathode material for calcium ion batteries *J. Electroanal. Chem.* **825** 51–6
[6] Dwivedi C, Mohammad T and Dutta V 2018 Creation of Au nanoparticles decorated MoO_3 nanorods using CoSP and the application as hole transport layer (HTL) in plasmonic-enhanced organic photovoltaic devices *Sol. Energy* **176** 22–9
[7] Li Z, Song P, Yang Z and Wang Q 2018 *In situ* formation of one-dimensional $CoMoO_4$/MoO_3 heterojunction as an effective trimethylamine gas sensor *Ceram. Int.* **44** 3364–70
[8] Behera B and Chandra S 2016 An innovative gas sensor incorporating ZnO–CuO nanoflakes in planar MEMS technology *Sensors Actuators B* **229** 414–24
[9] Munasinghe Arachchige H M M, Zappa D, Poli N, Gunawardhana N and Comini E 2018 Gold functionalized MoO_3 nano flakes for gas sensing applications *Sensors Actuators B* **269** 331–9
[10] Inpan U, Leangtanom P, Phokharatkul D, Wisitsoraat A, Phanichphant S and Kruefu V 2019 H2S gas sensor based on Ru-MoO_3 nanoflake thick film *J. Nanosci. Nanotechnol.* **19** 1780–5
[11] Yang S, Lei G, Lan Z, Xie W, Yang B, Xu H and Gu H 2019 Enhancement of the room-temperature hydrogen sensing performance of MoO3 nanoribbons annealed in a reducing gas *Int. J. Hydrogen Energy* **44** 7725–33
[12] Comini E, Yubao L, Brando Y and Sberveglieri G 2005 Gas sensing properties of MoO_3 nanorods to CO and CH_3OH *Chem. Phys. Lett.* **407** 368–71
[13] Comini E, Faglia G, Sberveglieri G, Cantalini C, Passacantando M, Santucci S and Qu W 2000 Carbon monoxide response of molybdenum oxide thin films deposited by different techniques *Sensors Actuators B* **68** 168–74
[14] Galatsis K, Li Y, Wlodarski W, Comini E, Faglia G and Sberveglieri G 2001 Semiconductor MoO_3–TiO_2 thin film gas sensors *Sensors Actuators B* **77** 472–7
[15] Hou L, Zhang C, Li L, Du C, Li X, Kang X-F and Chen W 2018 CO gas sensors based on p-type CuO nanotubes and CuO nanocubes: Morphology and surface structure effects on the sensing performance *Talanta* **188** 41–9
[16] Ferroni M, Guidi V, Martinelli G, Sacerdoti M, Nelli P and Sberveglieri G 1998 MoO_3-based sputtered thin films for fast NO_2 detection *Sensors Actuators B* **48** 285–8
[17] Prasad A K, Kubinski D J and Gouma P I 2003 Comparison of sol–gel and ion beam deposited MoO_3 thin film gas sensors for selective ammonia detection *Sensors Actuators B* **93** 25–30
[18] Rahmani M B, Keshmiri S H, Yu J, Sadek A Z, Al-Mashat L, Moafi A and Kalantar-zadeh K 2010 Gas sensing properties of thermally evaporated lamellar MoO_3 *Sensors Actuators B* **145** 13–9
[19] Poloju M, Jayababu N and Ramana Reddy M V 2018 Improved gas sensing performance of Al doped ZnO/CuO nanocomposite based ammonia gas sensor *Materials Science and Engineering: B* **227** 61–7
[20] Pisarkiewicz T, Stobinski L, Maziarz W, Michon D, Malolepszy A and Rydosz A 2018 *Gas Sensing Properties of Reduced Graphene Oxide Modified by Copper Oxide. 2018 XV Int. Scientific Conf. on Optoelectronic and Electronic Sensors (COE)* (https://doi.org/10.1109/coe.2018.8435159)
[21] Deshmane V V and Patil A V 2018 Structural and electrical properties of synthesized undoped iron oxide films *IJCPS* **7** 425–30

[22] Deshmane V V and Patil A V 2019 Study of In_2O_3 and α-Fe_2O_3 nano-composite as a petrol vapor sensor *Material Research Express* **6** 025904
[23] Deshmane V V and Patil A V 2019 Synergy of semiconductor (Hematite) and catalytic (Ni) properties enhance gas sensing behavior to NO2 *Mater. Res. Express* **6** 072910
[24] Epifani M, Imperatori P, Mirenghi L, Schioppa M and Siciliano P 2004 Synthesis and characterization of MoO3 thin films and powders from a molybdenum chloromethoxide *Chem. Mater.* **16** 5495–501
[25] Zhou J Y, Bai J L, Zhao H, Yang Z Y, Gu X Y, Huang B Y and Xie E Q 2018 Gas sensing enhancing mechanism via doping-induced oxygen vacancies for gas sensors based on indium tin oxide nanotubes *Sensors Actuators B* **265** 273–84
[26] Rosso K M, Smith D M A and Dupuis M 2003 An ab initio model of electron transport in hematite (α-Fe_2O_3) basal planes *J. Chem. Phys.* **118** 6455–66
[27] Singh J, Kaur G and Rawat M 2016 A brief review on synthesis and characterization of copper oxide nanoparticles and its applications *J Bioelectron Nantechnol* **1**
[28] Wang W-W, Du P-P, Zou S-H, He H-Y, Wang R-X, Jin Z and Yan C-H 2015 Highly dispersed copper oxide clusters as active species in copper-ceria catalyst for preferential oxidation of carbon monoxide *ACS Catalysis* **5** 2088–99
[29] Hou L, Zhang C, Li L, Du C, Li X, Kang X-F and Chen W 2018 CO gas sensors based on p-type CuO nanotubes and CuO nano-cubes: morphology and surface structure effects on the sensing performance *Talanta* **188** 41–9
[30] MunasingheArachchige H M M, Zappa D, Poli N, Gunawardhana N and Comini E 2018 Gold functionalized MoO_3 nano flakes for gas sensing applications *Sensors Actuators B* **269** 331–9